

Surface-plasmonic right-angle waveguide amplifiers

Jianhua JI^{1*}, Guirong ZHANG¹, Ke WANG¹, Ming XU¹,
Lu SUN^{1,2} & Chun JIANG^{1,2}

¹College of Information Engineering, Shenzhen University, Shenzhen 518060, China;

²State Key Laboratory of Advanced Optical communication Systems and Networks,
Shanghai Jiao Tong University, Shanghai 20040, China

Received 9 April 2017/Revised 19 June 2017/Accepted 1 August 2017/Published online 20 November 2017

Abstract We propose a surface-plasmonic right-angle bend waveguide with bismuth ion-doped glass film as core layer and Ag films as cladding layers for first time, to the best of our knowledge. Theoretical analysis shows that the right-angle has bend and absorption losses of 3.17 dB. The rate equations and power evolution equations of high concentration bismuth-doped glass film are setup and solved to analyze the effect of the waveguide length and active ion concentration on the signal gain and Noise Figure (NF). The theoretical results predict that with the pump power 100 mW, the active ion concentration 2.0×10^{26} ions/m³ and the right-angle waveguide size 1.0 cm × 1.0 cm, small-signal unit-length net gain can reach 15.32 dB with NF less than 5.0 dB.

Keywords surface-plasmonic, right-angle waveguide, bismuth ion-doped glass film, gain and noise figure, unit-length gain

Citation Ji J H, Zhang G R, Wang K, et al. Surface-plasmonic right-angle waveguide amplifiers. *Sci China Inf Sci*, 2018, 61(6): 062403, doi: 10.1007/s11432-017-9192-5

1 Introduction

Photonic integration is development trend of optical fiber communication systems and networks [1–3]. Ultracompact optical amplifiers are key devices of integrated optical communication subsystem such as optical add-drop multiplexers and optical cross-connecters. To make the amplifiers compact, the gain medium lengths have to be short, thus high concentration doping of active ions is necessary for compensation of short pump-signal interaction length, but the luminescent quenching effect of active ions in highly doped medium considerably degrades the gain of the devices. On the other hand, to realize the large-scale integration of photonic devices and subsystem, bend waveguide were widely investigated. Low-loss photonic-crystal waveguide bends were analyzed and optimized by the finite-difference time-domain method, semivectorial finite-difference method and supercell technique [4–6]. Ref. [7] reported the design and fabrication of a bend waveguide on 4.0 μm thick SOI with 1.27 μm effective radii and 0.09 dB loss. Ref. [8] reported a low-loss 90° waveguide bend composed of clothoid, and the bending loss with the bending radius of 4.0 μm has 90% reduction compared with normal bend. In a buried dielectric waveguide, waveguide core location could be adjusted to suppress a leaky wave so that pure bend and transition losses can be reduced [9]. A bent embedded waveguide with a loaded metal film was proposed to generate the surface plasmon-polariton mode for the transverse-magnetic wave [10]. In

* Corresponding author (email: jjh@szu.edu.cn)

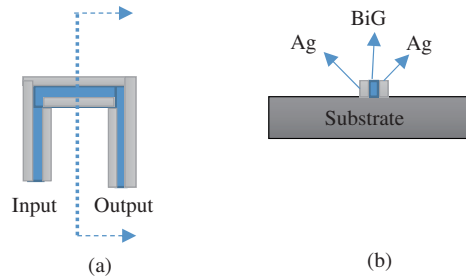


Figure 1 (Color online) A waveguide structure with bismuth-doped glass film (BiG) as core layer and Ag films as cladding layers. (a) Principal view; (b) cutaway view.

the waveguide, a low polarization dependent loss could be obtained over a wide spectral range. A two-dimensional photonic-crystal waveguide was proposed along with careful engineering of the individual cell at the corner to alleviate huge bending losses of a right-angle waveguide [11]. Ref. [12] designed a hybrid plasmonic waveguide with guided mode confined mainly into outer high-index slab, and the waveguide consisted of 5 nm-thick Au stripe and flexible multiple polymer cladding layers, the radiation loss due to bending was greatly suppressed. An SOI waveguide core size (440 nm \times 220 nm) was proposed with a bending radius of 1.0 μ m and substrate multilayers of Si/SiO₂, the bending loss reduction of the quasi-TM-mode up to \sim 2.5 dB/90° [13]. Ref. [14] investigated the effect of dielectric cladding on the waveguiding characteristics of an array of metallic pillars on a metal plane in the sub-terahertz band, and it was shown that by proper design of the dielectric medium surrounding the metallic structure the modal field confinement could be enhanced in a broad frequency band resulting in a low bending loss. In [15] authors designed and experimentally demonstrated a silicon slot waveguide operating at 1064 nm, and the transmission loss and bending loss were measured as 6.0 dB/cm and 4.1 dB/180°. A polarization rotator based on a bend asymmetric-slab waveguide on the silicon-on-insulator platform was recently reported [16] with ultracompact structure of \sim 5.0 μ m conversion length and an insertion loss of 0.5 dB and an extinction ratio of $>$ 40.0 dB for both TE to TM polarization conversion and TM to TE polarization conversion.

Additionally, in recent years, bismuth ion-doped glasses, which have broadband emission spectrum covering from 1100–1700 nm, are promising for broadband fiber amplifiers. However, the concentration quenching induced by up-conversion and excited state absorption still appears in high-concentration bismuth ion doped media. Up to now, the gain and noise figure of high concentration bismuth-doped waveguide amplifiers have not been studied.

In this work, we will explore the possibility of rare-earth-doped bend waveguide for compact integrated devices and integrated photonic system. As an active waveguide, rare-earth-doped bend waveguide will be used to integrated photonic devices and photonic system. We use the metal-insulator-metal (MIM) waveguide to confine the pump light and signal light fields within the waveguide core to enhance light-matter interaction, and we also try to reduce the bend loss using surface-plasmonic waveguide. Thus, we propose a surface-plasmonic right-angle waveguide with bismuth ion-doped glass film as core layer and Ag films as cladding layers. A numerical model of bismuth ion waveguide amplifier incorporating excited state absorption and cooperative up-conversion into rate equations and power evolution equations, and we solve the equation groups to analyze the effect of active ion concentration and waveguide length on the amplifier gain and noise figure.

2 Waveguide structure design and theoretical analysis

Figure 1 shows the schematic of the right-angle bend waveguide structure, which uses bismuth-doped glass film as core layer and metal Ag film as cladding layers. The structure below the waveguide is substrate which is used to support the Ag and Bi⁺-doped glass films (BiG), where the Figure 1(b) is the cross section of the Figure 1(a).

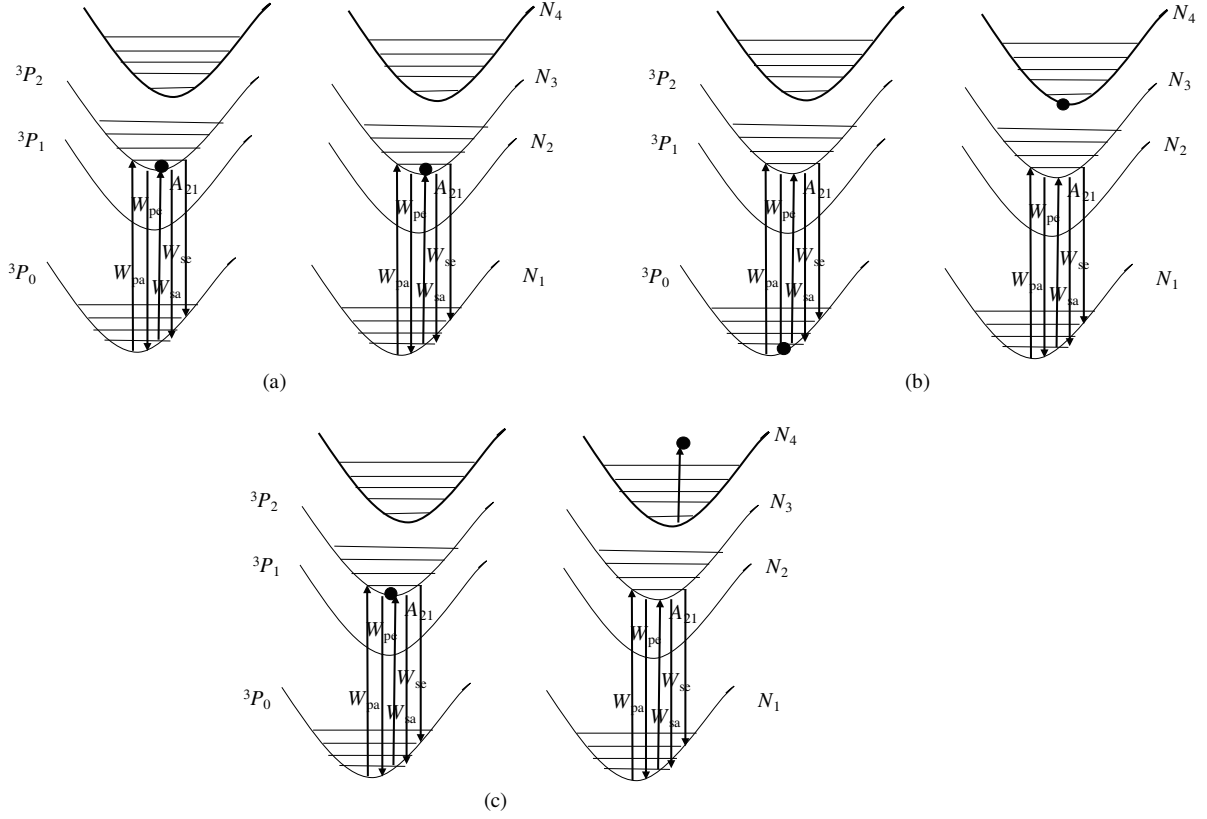


Figure 2 Schematic coordination configuration energy levels of bismuth-doped glass with excited state absorption. (a) Two electrons are excited to 3rd-levels; (b) one electron transits to ground level and other is excited to 4th-level; (c) one electron is excited to 3rd-level and other is excited to higher level.

Figure 2 shows the schematic energy levels of a Bi^{3+} -doped $60\text{SiO}_2\text{-}30\text{Al}_2\text{O}_3\text{-}9\text{La}_2\text{O}_3\text{-}1\text{Bi}_2\text{O}_3$ system [17]. With 980 nm excitation, electrons are excited to the third level (3P_2) from the ground state (3P_0), then nonradiatively relax to the second level (3P_1). The electrons at 3P_1 level transit to the ground state (3P_0), emitting 1000–1600 nm photons. With higher dopant concentration, the distance between neighboring Bi^{3+} ions is so short that the two Bi^{3+} ions in second level may form an ion pair (Figure 2(a)). In this pair, the electron of one of two Bi^{3+} ions transits to the ground state, and the electron of the other Bi^{3+} ion is excited to the fourth level (Figure 2(b)) and then nonradiatively relaxes to the third level, and is then excited again to higher level by absorbing one 980 nm pump photon (Figure 2(c)). Following this diagram, the rate equations can be written as 3P_1 .

$$\frac{dN_1}{dt} = -(W_{12} + W_{13} + W_{14})N_1 + (W_{21} + A_{21} + C_u N_2)N_2 + (W_{31} + A_{31})N_3 + (W_{41} + A_{41})N_4, \quad (1)$$

$$\frac{dN_2}{dt} = W_{12}N_1 - (W_{21} + A_{21} + 2C_u N_2)N_2 + A_{32}N_3, \quad (2)$$

$$\frac{dN_3}{dt} = W_{13}N_1 - (A_{32} + W_{31} + A_{31} + W_{34})N_3 + A_{43}N_4, \quad (3)$$

$$\frac{dN_4}{dt} = W_{14}N_1 + C_u N_2^2 - A_{43}N_4. \quad (4)$$

In these equations the W_{ij} terms represent the stimulated transition rates between i and j levels, A_{ij} terms represent the spontaneous transition rates from i to j level. C_{up} is the cooperative upconversion coefficients of active ion pair. The total distributions N of active ion density is assumed to be constant within the whole waveguide cross-section and along the waveguide length. It satisfies the conservation equation

$$N = N_1 + N_2 + N_3 + N_4. \quad (5)$$

Propagation of the pump power along the waveguide is described by the following differential equation:

$$\frac{dP_p}{dz} = -[\Gamma_p(N_1\sigma_{13} - N_3\sigma_{31} + N_3\sigma_{34}) + \alpha_p]P_p. \quad (6)$$

The signal power and ASE powers are amplified according to

$$\frac{dP_s}{dz} = [\Gamma_s(N_2\sigma_{21} - N_1\sigma_{12}) - \alpha_s]P_s, \quad (7)$$

$$\frac{dP_s}{dz} = [\Gamma_s(N_2\sigma_{21} - N_1\sigma_{12}) - \alpha_s]P_s, \quad (8)$$

where $\alpha(\nu)$ is the frequency-dependent background loss of the active fiber and σ_{ij}, σ_{ji} are the corresponding emission and absorption cross sections between i and j level. Γ_k ($k = p, s, ase$) is overlap integration between pump, signal, spontaneous and Bi⁺ ion distribution.

Eqs. (6)–(8) form a system of coupled differential equations, which are solved by numerical integration along the active waveguide by using Matlab programming and Newton-iteration algorithm and Rung-Kutta algorithm. It was assumed that the up-conversion coefficient C_u is linearly increasing functions of N [18,19]

$$C_u = 3.50 \times 10^{-24} + 2.41 \times 10^{-49}(N - 4.4 \times 10^{25}). \quad (9)$$

Then the gain can be calculated by the following equation:

$$G \text{ (dB)} = 10 \log_{10} (P_o/P_i), \quad (10)$$

where P_i, P_o are the power at input and output ends of the waveguide, respectively.

Noise figure is key performance of an amplifier and can be calculated using Giles model [20]:

$$\text{NF (dB)} = 10 \log_{10} (1/G + P_{ase}/(Gh\nu\Delta\nu)). \quad (11)$$

3 Result and discussion

3.1 Simulation parameters

Table 1 is the spectroscopic parameters of the bismuth-doped glass [21,22]. In the references the absorption coefficient and absorption cross sections at the wavelength 1530 nm are 17.0 cm^{-1} , $8.0 \times 10^{-20} \text{ cm}^2$, respectively. According to the relation between absorption and emission cross sections, the calculated emission cross section at 1530 nm is closed to $8.0 \times 10^{-20} \text{ cm}^2$. The absorption coefficient and absorption cross section at the pump wavelength 980 nm was 16.0 cm^{-1} , $9.0 \times 10^{-20} \text{ cm}^2$, and the calculated emission cross section is closed to $9.0 \times 10^{-20} \text{ cm}^2$. It is assumed that the 3P_1 excited state absorption cross section at 980 nm is same as the ground state absorption cross section, the spontaneous transition probabilities A_{21}, A_{31}, A_{41} , and A_{32} are listed in Table 1. Additionally, in this work it is assumed that the waveguide core width is 1.0 μm , and the bismuth ion distribution is uniform in the waveguide cross section, and the overlaps between the mode fields of ASE at 500 nm, ASE at 700 nm and bismuth ion distribution approximately equal to 0.4, and the overlaps between the mode fields of 980 nm pump and 1530 nm signal and active ion distribution approximately equal to 0.7, 0.8, respectively.

3.2 Right-angle bend waveguide loss

Finite-difference time-domain method (FDTD) is used to calculate the transmission, reflection and loss spectra of the right-angle waveguide. The electrical field polarization, which is parallel to the propagation plane, is used as a launching source. The size of two-dimensional computation cell is 4 a \times 4 a, and numerical resolution is 150 point/a \times 150 point/a, thus the grid of the entire computation cell is 600 point \times 600 point, and the length of the right-angle waveguide is 4 a, the thickness of the perfectly matched layer is 0.5 a, and the current source is Gaussian pulse in time and its normalized center frequency is 3.0 (c/a) and frequency width is 0.8 (c/a), where ‘a’ is an arbitrary unit, ‘c’ is speed of light

Table 1 Spectroscopic parameters of bismuth ion-doped glasses

Description	Parameters value (unit)
Pump /signal wavelength (λ_p/λ_s)	980 nm/1530 nm
Absorption/emission cross section @980 nm	$9.0 \times 10^{-26} \text{ m}^2 / 9.0 \times 10^{-26} \text{ m}^2$
Excited state absorption cross section @980 nm	$9.0 \times 10^{-26} \text{ m}^2$
Absorption /emission cross section @1530 nm	$8.0 \times 10^{-26} \text{ m}^2 / 8.0 \times 10^{-26} \text{ m}^2$
Absorption/emission cross section @700 nm	$3.33 \times 10^{-26} \text{ m}^2 / 3.33 \times 10^{-26} \text{ m}^2$
Absorption/emission cross section @500 nm	$8.31 \times 10^{-25} \text{ m}^2 / 8.31 \times 10^{-25} \text{ m}^2$
$A_{21} (\text{Bi}^+ \ ^3P_1 \ ^3P_0)$	1000/5.0/s
$A_{31} (\text{Bi}^+ \ ^3P_2 \ ^3P_0)$	10000/s
$A_{41} (\text{Bi}^+ \ ^3P_3 \ ^3P_0)$	1000000/230/s
$A_{32} (\text{Bi}^+ \ ^3P_2 \ ^3P_1)$	1000000/s
Waveguide core width, height	1.0 μm
Overlap @1530 nm	0.8
Overlap @980 nm	0.6
Overlap @500 nm, 700 nm	0.4

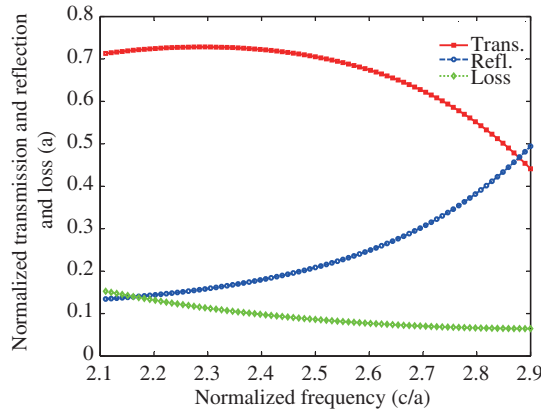


Figure 3 (Color online) Transmission, reflection and loss spectra of un-doped MIM right-angle waveguide calculated using FDTD method. ‘a’ is an arbitrary unit, ‘c’ is speed of light.

in vacuum. The pulse is launched at the input end of the waveguide, and the fields are monitored at input and output ends. Figure 3 shows the transmission, reflection and loss spectra of un-doped MIM right-angle waveguide. It is shown from Figure 3 that the highest transmission occurs around the normalized frequency 2.3 (c/a), the right-angle transmission is 73%, corresponding loss is 3.17 dB, including bend loss and absorption loss caused by surface-plasmon. If the signal wavelength is 1530 nm, then $a=2.3 \times 1530 \text{ nm}=3.519 \mu\text{m}$, and the pump wavelength 1480 nm corresponds to the normalized frequency 2.38 (c/a), the right-angle bend transmission is 72%, corresponding loss is 3.12 dB.

3.3 Effect of waveguide length on gain and noise figure

Figure 4 shows the dependence of small-signal gain and noise figure on waveguide length. Bismuth ion concentration is $2.0 \times 10^{26} /\text{m}^3$, pump power is 100.0 mW. The results demonstrate that the gain linearly increases with waveguide length when the length is shorter than 8.0 cm, and the gain begins to saturate at the length 8.0 cm and the saturation value is 28.0 dB. The noise figure increases with waveguide length when the length is shorter than 2.0 cm, and the noise figure begins to saturate at the length 2.0 cm and the saturation value is 4.2 dB.

3.4 Effect of active ion concentration on gain and noise figure

Figure 5 illustrates the variation of small-signal gain and noise figure with bismuth ion concentration. In

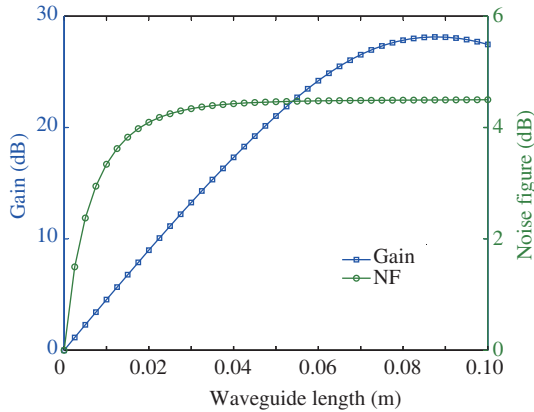


Figure 4 (Color online) Dependence of small-signal gain of bismuth-doped glass waveguide amplifier on waveguide length. Doping concentration, pump power, signal wavelength and signal input power are $2.0 \times 10^{26} / \text{m}^3$, 100 mW, 1532 nm and 1.0 μW , respectively.

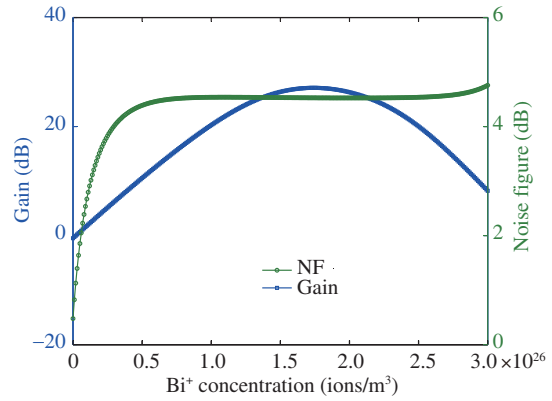


Figure 5 (Color online) Variation of small-signal gain and noise figure of bismuth ion-doped waveguide amplifier on bismuth ion concentration. waveguide length, pump power, signal wavelength and signal input power are 10.0 cm, 100 mW, 1532 nm and 1.0 μW , respectively.

Table 2 Doping concentrations and internal gain and gain per unit length of surface-plasmonic bismuth ion-doped right-angle glass waveguide amplifier and erbium and ytterbium co-doped phosphate fiber amplifier ^{a)}

Pumping power/ Fiber length	Optimal erbium/ytterbium concentration (ion/m^3)	Gain (dB)	Gain/cm (dB/cm)	Reference
224 mW/3.6 cm	4.0×10^{26} , 8.0×10^{26}	31.0	8.61	[22]
224 mW/5.55 cm	3.0×10^{26} , 8.0×10^{26}	35.0	6.31	[22]
Pump power/wave- guide length	Bismuth ion concentration	Gain	Gain/cm	This work
100 mW/8.0 cm	2.0×10^{26}	28.0	15.32	

a) Signal wavelength is 1535 nm, and signal input power is -30 dBm.

this calculation, waveguide length is 10.0 cm, pump power is 100 mW, and signal wavelength and power is 1532 nm and 1.0 μW , respectively. The results show that the gain of the amplifier increases as bismuth ion concentration and reaches the saturation value 28.0 dB near $1.7 \times 10^{26} \text{ ions}/\text{m}^3$. With same parameters as above, the NF increases until the active ion concentration reaches $5.0 \times 10^{25} \text{ ion}/\text{m}^3$, then it stops increasing to reach the saturation value 4.4–4.5 dB.

3.5 Amplifier size and unit-length gain

It is known from Figure 4, when the waveguide length is 8.0 cm, the gain reaches the maximum 28.00 dB. If the on-chip amplifier includes one right-angle, the size is 4.0 cm \times 4.0 cm, then the net gain is 28.00–3.17=24.83 (dB). If it includes two right-angles, the size is 2.7 cm \times 2.7 cm, if it includes four right-angles, the size is 1.0 cm \times 1.0 cm, the net gain is 28.0–4 \times 3.17=15.32 (dB). In [23], erbium-doped fiber amplifiers used pump power (224 mW/980 nm) and different fiber length, optimal erbium and ytterbium co-doping concentration, internal gain and gain per unit length are listed in Table 2. For the fiber length of 3.6 cm, optimal erbium and ytterbium co-doping concentration are $4.0 \times 10^{26} / \text{m}^3$, $8.0 \times 10^{26} / \text{m}^3$, respectively. For the fiber length of 5.55 cm, optimal erbium and ytterbium co-doping concentration are $3.00 \times 10^{26} / \text{m}^3$, $8.0 \times 10^{26} / \text{m}^3$, respectively. The gain reach 35.0 dB and gain per centimeter reach 5.68 dB/cm. In our present work, pump power 100 mW and active ion concentration $2.00 \times 10^{26} / \text{m}^3$, the gain medium length 8.0 cm with four right angles, corresponding to the waveguide size 1.0 cm \times 1.0 cm, the gain can reach 28.0 dB, that is, the gain per unit waveguide length is 15.32 dB/cm, which is the largest value for gain per unit length, to the best of our knowledge. We think, compared with the phosphate glass fiber amplifier, the advantage of surface-plasmonic right-angle bismuth ion doped-glass waveguide amplifier arises from smaller size.

4 Conclusion

As a summary, we designed a surface-plasmonic right-angle bend waveguide with bismuth ion-doped glass film as core layer and Ag films as cladding layers. Theoretical analysis showed that the right-angle bend has bend and absorption losses of 3.17 dB. The rate equations and power evolution equations of high concentration bismuth-doped glass film were setup and solved to analyze the effect of the waveguide length and active ion concentration on the signal gain and NF. The theoretical results show that with the pump power 100 mW, the active ion concentration 2.0×10^{26} ions/m³ and the right-angle bend waveguide 1.0 cm \times 1.0 cm, small-signal unit-length gain can reach 15.32 dB with NF less than 5.0 dB. This waveguide amplifier will be promising for integrated photonic devices and optical communication subsystem.

Acknowledgements This work was supported by National Natural Science Foundation of China (Grant Nos. 60377023, 61671306) and Science and Technology Innovation Commission of Shenzhen (Grant No. JCYJ20160328-145357990).

Conflict of interest The authors declare that they have no conflict of interest.

References

- 1 Wang Q M. Investigation progress on key photonic integration for application in optical communication network. *Sci China Ser F-Inf Sci*, 2003, 46: 60–66
- 2 Ji Y F, Zhang J W, Zhao Y L, et al. Prospects and research issues in multi-dimensional all optical networks. *Sci China Inf Sci*, 2016, 59: 101301
- 3 Guo P X, Hou W G, Guo L. Designs of low insertion loss optical router and reliable routing for 3D optical network-on-chip. *Sci China Inf Sci*, 2016, 59: 102302
- 4 Zheng W H, Xing M X, Ren G, et al. Integration of a photonic crystal polarization beam splitter and waveguide bend. *Opt Express*, 2009, 17: 8657–8668
- 5 Che M, Li Z Y. Light propagation through two-dimensional photonic crystal slab waveguide bends solved by three-dimensional plane-wave transfer-matrix method. *J Opt Soc Am B*, 2009, 26: 493–498
- 6 Dai D X, He S L. Analysis of characteristics of bent rib waveguides. *J Opt Soc Am A*, 2004, 21: 113–121
- 7 Cherchi M, Ylino S, Harjanne M, et al. Dramatic size reduction of waveguide bends on a micron-scale silicon photonic platform. *Opt Express*, 2013, 21: 17814–17823
- 8 Fujisawa T, Makino S, Sato T, et al. Low-loss, compact, and fabrication-tolerant Si-wire 90° waveguide bend using clothoid and normal curves for large scale photonic integrated circuits. *Opt Express*, 2017, 25: 9150–9159
- 9 Nito Y, Yatabe B, Yamauchi J, et al. Reduction in bend losses of a buried waveguide on a silicon substrate by adjusting the core location. *J Lightwave Technol*, 2016, 34: 1344–1349
- 10 Nito Y, Kadowake D, Yamauchi J, et al. Bent embedded optical waveguide with a loaded metal film for reducing a polarization dependent loss. *J Lightwave Technol*, 2013, 31: 3195–3202
- 11 Kurt H, Giden I H, Ustun K. Highly efficient and broadband light transmission in 90° nanophotonic wire waveguide bends. *J Opt Soc Am B*, 2011, 28: 495–501
- 12 Jin T K, Park S, Ju J J, et al. Low bending loss characteristics of hybrid plasmonic waveguide for flexible optical interconnect. *Opt Express*, 2010, 18: 24213–24220
- 13 Serpa C, Hernandez-Figueroa H E. Reduction of bending loss for the TM mode in a strip-waveguide using a metamaterial in SOI-based platform. In: *Proceedings of Latin America Optics and Photonics Conference, Medellin*, 2016
- 14 Moghaddam M A, Ahmadi-Boroujeni M. Design of a hybrid spoof plasmonic sub-terahertz waveguide with low bending loss in a broad frequency band. *Opt Express*, 2017, 25: 6860–6873
- 15 Li X D, Feng X, Huang Y D. Silicon slot waveguide with low transmission and bending loss at ~ 1 μm . In: *Proceedings of Asia Communications and Photonics Conference, Hong Kong*, 2015
- 16 Cao T T, Chen S W, Fei Y H, et al. Ultra-compact and fabrication-tolerant polarization rotator based on a bend asymmetric-slab waveguide. *Appl Opt*, 2013, 52: 990–996
- 17 Meng X-G, Qiu J-R, Peng M-Y, et al. Near infrared broadband emission of bismuth-doped aluminophosphate glass. *Opt Express*, 2005, 13: 1628–1634
- 18 Delevaque E, Georges T, Monerie M, et al. Modeling of pair-induced quenching in erbium-doped silicate fibers. *IEEE Photonic Tech L*, 1993, 5: 73–75
- 19 Myslinski P, Nguyen D, Chrostowski J. Effects of concentration on the performance of erbium-doped fiber amplifiers. *J Lightwave Technol*, 1997, 15: 112–120
- 20 Giles C R, Desurvire E. Modeling erbium-doped fiber amplifiers. *J Lightwave Technol*, 1991, 9: 271–283
- 21 Dvoyrin V V, Kir'yanov A V, Mashinsky V M, et al. Absorption, gain, and laser action in bismuth-doped aluminosilicate optical fibers. *IEEE J Quantum Elect*, 2009, 46: 182–190
- 22 Qian M, Cheng J M, Hu L L. Dependence of spectroscopic properties on doping content and temperature of bismuth-doped lanthanum aluminosilicate glass. *Chin Opt Lett*, 2012, 10: 111602
- 23 Hu Y, Jiang S, Luo T, et al. Performance of high-concentration Er/sup 3+/-Yb/sup 3+/-codoped phosphate fiber amplifiers. *IEEE Photonic Tech L*, 2001, 13: 657–659